Featured Article

Noninvasive Magnetic Resonance Spectroscopic Imaging Biomarkers to Predict the Clinical Grade of Pediatric Brain Tumors

Loukas G. Astrakas,[1] David Zurakowski,[2,3] A. Aria Tzika,[1] Maria K. Zarifi,[1] Douglas C. Anthony,[6] Umberto De Girolami,[4] Nancy J. Tarbell,[7] and Peter McLaren Black[5]

[1]Nuclear Magnetic Resonance Surgical Laboratory, Department of Surgery, Massachusetts General Hospital, Shriners Burns Institute, Harvard Medical School, Boston, Massachusetts; Departments of [2]Biostatistics, [3]Orthopaedic Surgery, [4]Pathology, and [5]Neurosurgery, Children's Hospital, Harvard Medical School, Boston, Massachusetts; [6]Department of Pathology and Anatomical Sciences, University of Missouri-Columbia, Columbia, Missouri; and [7]Department of Radiation Oncology, Massachusetts General Hospital, Harvard Medical School, Boston, Massachusetts

ABSTRACT

The diagnosis and therapy of childhood brain tumors, most of which are low grade, can be complicated because of their frequent adjacent location to crucial structures, which limits diagnostic biopsy. Also, although new prognostic biomarkers identified by molecular analysis or DNA microarray gene profiling are promising, they too depend on invasive biopsy. Here, we test the hypothesis that combining information from biologically important intracellular molecules (biomarkers), noninvasively obtained by proton magnetic resonance spectroscopic imaging, will increase the diagnostic accuracy in determining the clinical grade of pediatric brain tumors. We evaluate the proton magnetic resonance spectroscopic imaging exams for 66 children with brain tumors. The intracellular biomarkers for choline-containing compounds (Cho), *N*-acetylaspartate, total creatine, and lipids and/or lactate were measured at the highest Cho region and normalized to the surrounding healthy tissue total creatine. Neuropathological grading was done with WHO criteria. Normalized Cho and lipids and/or lactate were elevated in high-grade ($n = 23$) *versus* low-grade ($n = 43$) tumors, which multiple logistic regression confirmed are independent predictors of tumor grade (for Cho, odds ratio 24.8, $P < 0.001$; and for lipids and/or lactate, odds ratio 4.4, $P < 0.001$). A linear combination of normalized Cho and lipids and/or lactate that maximizes diagnostic accuracy was calculated by maximizing the area under the receiver operating characteristic curve. Proton magnetic resonance spectroscopic imaging, although not a proxy for histology, provides noninvasive, *in vivo* biomarkers for predicting clinical grades of pediatric brain tumors.

INTRODUCTION

Brain tumors in children are highly heterogeneous for histology, prognosis, and therapeutic response. The most common pediatric brain tumors, cerebellar astrocytomas, medulloblastomas, ependymomas, and brain stem gliomas, occur infratentorially, whereas malignant and benign astrocytomas and ependymomas are often supratentorial (1). Although most childhood brain tumors are low grade and respond to therapy, their diagnosis and treatment are often complicated by their frequent location adjacent to crucial structures to restrict diagnostic biopsies.

The paucity of biological markers with prognostic significance greatly limits the development of new treatment strategies, and their identification could allow a new accurate staging system and treatment better tailored to tumor characteristics and behavior. Although such markers may be identified through molecular analysis (2, 3) and DNA microarray gene profiling (4, 5), these procedures also require diagnostic biopsies that can be impeded by tumor location. In contrast, biologically relevant intracellular molecules or metabolites can be detected with noninvasive and nonirradiating, *in vivo* proton magnetic resonance spectroscopic imaging and potentially promise a new era in brain tumor management.

Advances in multivoxel proton magnetic resonance spectroscopic imaging allow the simultaneous collection of spectral data from multiple regions, including the tumor and its surroundings, to illuminate the spatial distribution of spectral changes. Brain tumor magnetic resonance spectroscopic imaging can predict histology, follow serial changes in tumor grade, corroborate responses to chemotherapy and/or radiation, and accurately differentiate tumor tissue from radiation necrosis, normal tissue, or other structural abnormalities (6–13). Brain tumor proton magnetic resonance spectroscopic imaging studies consistently show the reduction or absence *versus* control subjects of *N*-acetylaspartate (NAA) and total creatine, including creatine and phosphocreatine, likely due to edema and necrosis, an increase in choline-containing compounds (Cho), possibly via cell membrane disruption and altered phospholipid metabolism during rapid cell growth and neoplasia (14, 15), and increased lactate, reflecting metabolically active tumor cells (16). Reduced NAA is expected in tumors because it is primarily localized to healthy neurons (17, 18), and thus, observed NAA is either due to tumor infiltration of normal tissue or immature oligodendroglia or neoplastic alterations because NAA occurs in

Received 3/29/04; revised 9/2/04; accepted 9/17/04.
Grant support: American Cancer Society grant RPG-98-056-01-CCE. The costs of publication of this article were defrayed in part by the payment of page charges. This article must therefore be hereby marked *advertisement* in accordance with 18 U.S.C. Section 1734 solely to indicate this fact.
Requests for reprints: A. Aria Tzika, NMR Surgical Laboratory, Department of Surgery, Massachusetts General Hospital, Harvard Medical School, 51 Blossom Street, Room 261, Boston, MA 02114. Phone: (617) 371-4871; Fax: (617) 720-3544; E-mail: atzika@partners.org.

oligodendroglia progenitor cell cultures (19) and in human glial neoplasia precursors (20). Proton magnetic resonance spectroscopic imaging, with shorter echo times, can detect a special class of *in vivo* cell lipids via broad spectral peaks from lipids present in intracellular cytosolic (21, 22) and membrane vesicles, possibly in dynamic exchange. These peaks are especially prominent in proliferating and malignant cells (23). In cell cultures, the appearance of a lipid peak at 1.3 parts per million (ppm) from lipid moieties has been associated with apoptotic cell death *versus* necrosis or nonapoptotic cell death (24). In tumor tissues, lipids coincide with histopathologically proven necrosis (25, 26), although the role of proton magnetic resonance spectroscopic visible lipids in the apoptotic pathway is unclear. Nonetheless, such lipids likely contribute to tumor prognosis (27).

Here, we rigorously test our hypothesis that biologically important intracellular molecules illuminated by proton magnetic resonance spectroscopic imaging, including Cho and lipids/lactate, can aid the clinical grading of pediatric central nervous system tumors. We present and discuss the prognostic information provided by these biomarkers and show for the first time in pediatric brain tumors, that when used in combination, these biomarkers provide a more accurate prognosis.

PATIENTS AND METHODS

We studied 66 patients with pediatric brain tumors. Clinical data were obtained from the Children's Hospital (Boston, MA) tumor registry and from hospital charts. This data includes patient age at diagnosis and sex of the patient. The mean patient age at the time of diagnosis was 9.5 years. We included both sexes, 39 boys and 27 girls. Tumors were classified by the neuropathologists at Children's Hospital, with the current WHO histologic brain tumor classification, and Table 1 presents their histopathological breakdown. Each case was also reviewed by a single neuropathologist (D. Anthony) to confirm classification. Informed consent was obtained from the parent or guardian of each participant before inclusion if the study was not clinically indicated.

Table 1 Histopathologic breakdown of brain tumors

Histopathologic diagnosis	No. of cases	WHO
Craniopharyngioma	4	I
Dysembryoplastic neuroepithelial tumor	2	I
Ganglioglioma	2	I
Pilocytic astrocytoma	5	I
Astrocytoma	10	II
Brain stem glioma	7	II
Ependymoma	2	II
Mixed glioma	1	II
Oligodendroglioma	2	II
Optic glioma	1	II
Pontine glioma	6	II
Thalamic astrocytoma	1	II
Anaplastic astrocytoma	6	III
Anaplastic ependymoma	1	III
Choroid plexus carcinoma	1	IV
Desmoplastic medulloblastoma	1	IV
Glioblastoma multiforme	2	IV
Hypothalamic astrocytoma	1	IV
Medulloblastoma	3	IV
Pineoblastoma	1	IV
Poorly differentiated malignant neoplasm	3	IV
Poorly differentiated neuroectodermal tumor	1	IV
Rhabdoid tumor	2	IV
Supratentorial PNET	1	IV

Studies were done with conventional magnetic resonance imaging and proton magnetic resonance spectroscopic imaging before treatment on a General Electric 1.5-T magnetic resonance system (General Electric Medical System, Milwaukee, WI). Proton magnetic resonance spectroscopic imaging was done with multivoxel chemical shift imaging with point resolved spectroscopy and volume preselection (28). Shimming and water suppression were adjusted after selecting a 50 to 100 mL of volume. Water suppression was done with chemical shift selection and volume selection, with radiofrequency pulses of bandwidths of 1100 Hz for the 180° pulse and 2000 Hz for the 90° pulse. A large data set was acquired with phase-encoding gradients in two directions, with the following acquisition parameters: repetition time = 1 second, echo time = 65 milliseconds, 16 × 16 phase encoding matrix, 160-mm field of view, 10-mm slice thickness, 1250-Hz spectral width, two averages, and 512 points. Data sets of 1 to 1.2 mL of nominal resolution were obtained.

A 65-millisecond echo time was used to reduce contributions from lactate because we were primarily interested in detecting lipids. Most brain tumor magnetic resonance spectroscopic imaging studies have used an echo time of 270 or 272 milliseconds to detect lactate, however, our goal was to increase lipid sensitivity. The prominent peaks of biological importance were NAA at 2.0 ppm, Cho at 2.2 ppm, total creatine at 3.0 ppm, and lipids/lactate at 1.3 ppm. Data processing was performed on a Sun workstation (Sun Microsystems, Mountain View, CA) with General Electric spectroscopy analysis software (SAGE) and in-house software developed with Interactive Data Language 5.3 (Research Systems, Boulder, CO). The data sets were apodized with a 1.0-Hz Lorentzian filter, Fourier-transformed in the time domain and the two spatial domains, and phased with SAGE, first automatically and then manually, if necessary. A baseline estimator was then applied to subtract the broad components of the baseline before peak area calculations. Finally, the areas of selected metabolite peaks were estimated with the peak algorithm (29) developed in Interactive Data Language. Metabolite images were generated and stored as TIFF files on a Sun Sparc workstation, transferred to a Macintosh workstation, where imaging editing software, including NIH Image and Adobe PhotoShop, was used to overlay the metabolite images onto the corresponding anatomic images. Composite metabolite images (*i.e.,* Cho + lipids and/or lactate images) were created by adding the Cho and lipids and/or lactate values for every voxel and then assembling the result in a 0 to 255 red scale voxel image. The Cho + lipids and/or lactate voxel image was extrapolated then to the magnetic resonance imaging image scale (256 × 256) and superimposed on it.

Normalized magnetic resonance spectroscopic imaging variables for NAA, Cho, total creatine, and lipids and/or lactate, expressed in arbitrary units, were obtained by dividing their values from within tumor regions to the mean value of normal tissue total creatine, which serves as the internal standard in these patients (6). We obtained multiple measurements from

multiple voxels per patient to account for brain tumor heterogeneity with tumor size and resolution limiting factors.

To compare the histopathological and the magnetic resonance data, we performed the magnetic resonance spectroscopic imaging analysis with respect to the highest Cho region to mimic pathological evaluations derived from the most malignant area of the biopsy specimen. To spatially correlate the histopathological information with the magnetic resonance data, the surgeon collected biopsy specimens from within the volume of interest, as shown in the magnetic resonance images, and superimposed magnetic resonance spectroscopic imaging data set, which were brought to the operating room. In certain cases, the surgeon obtained biopsy samples with the guidance of a surgical navigation system to determine the location of each biopsy site on the magnetic resonance images. To this end, immediately before removal of a biopsy specimen, a multiplanar magnetic resonance image of the origin of the sample was saved by using an ISG Viewing Wand (ISG Technologies, Mississauga, Ontario, Canada). Each sample was then obtained with small surgical forceps, labeled, and individually submitted for routine pathological examination.

Biostatistical Methods. Patients were classified according to tumor grade with WHO I or II defined as low grade, and WHO III or IV as high grade. The nonparametric Mann-Whitney *U* test was used to compare patients with high-grade *versus* low-grade tumors, with respect to median values of Cho and lipids and/or lactate. Predictive diagnostic characteristics of sensitivity and specificity were calculated with standard formulas, which define sensitivity as the frequency of a positive test result in those patients with high-grade tumors, and specificity as the frequency of a negative test result in those with low-grade tumors (30). Multiple stepwise logistic regression analysis was done to evaluate whether Cho and lipids and/or lactate were independent predictors of tumor grade. The logistic regression equation includes coefficients, SEs, adjusted odds ratios, 95% confidence intervals, and the likelihood ratio χ^2 test for parameters in the final model obtained by maximum likelihood estimation (31). The probability of a high-grade tumor was estimated for a range of predictor combinations.

To achieve optimal diagnostic accuracy we applied the distribution-free method of Pepe and Thomas (32), the linear combination of Cho and lipids and/or lactate that maximizes the area under the receiver operating characteristic (ROC) curve. The ROC curve plots sensitivity (*Y* axis) *versus* one-specificity (*X* axis) or false positive rate with the points on the curve generated with the cutoff values of the predictors (33). Area under the ROC curve (AUC) is the most widely used index for diagnostic accuracy. The AUC was estimated nonparametrically and used as a measure of test accuracy (34). The likelihood ratio was defined as sensitivity (one-specificity) AUCs were compared with the Z test, as described previously (35). Statistical analysis was conducted with the SPSS software package (version 12.0, SPSS Inc., Chicago, IL), and two-tailed *P* values of <0.05 were considered statistically significant.

RESULTS

Fig. 1 shows magnetic resonance images and spectra from a representative patient with a low-grade supratentorial pediatric brain tumor located at the level of the basal ganglia. Three prominent peaks of biologically significant compounds, NAA, total creatine, and Cho, are well resolved from each other and dominate the magnetic resonance spectral patterns. The figure illustrates a mismatch of contrast enhancement, T2 signal ab-

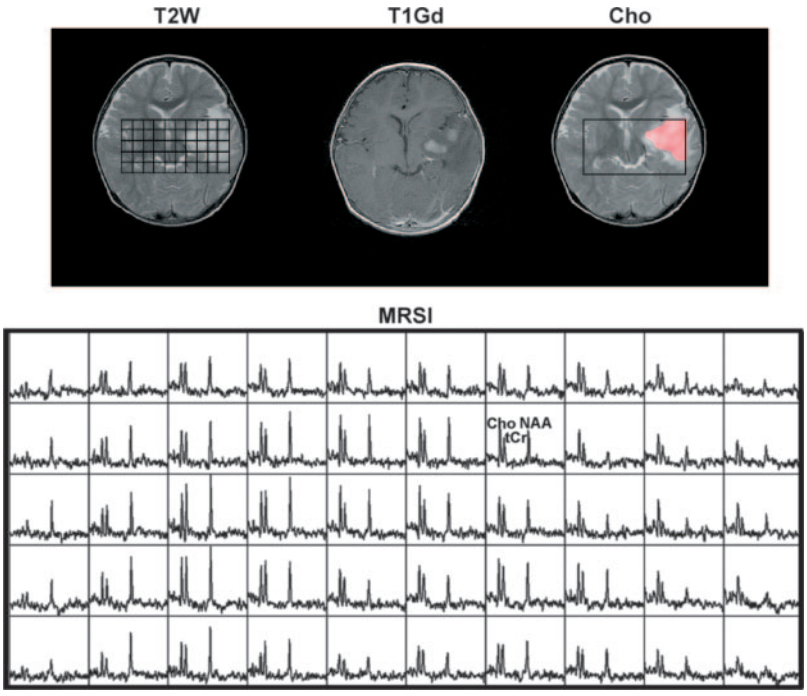

Fig. 1 Magnetic resonance imaging and proton magnetic resonance spectroscopic imaging (MRSI) on a 2-year-old boy with low-grade astrocytoma. T2W, T2-weighted image; T1Gd, gadolinium-enhanced image; and Cho, choline metabolite map overlaid on the T2W image. The lesion appears inhomogeneously hyperintense on the T2W image and fails to completely enhance on the T1W image. The grid overlay on the T2W image shows the anatomic locations for the simultaneous MRSI spectral acquisitions from multiple locations in one slice. Note the mismatch of contrast enhancement on the T1W image, T2 signal abnormality on the T2W image, and elevated Cho on the Cho metabolite image. In this case, Cho by MRSI may be a more inclusive biomarker, *versus* contrast enhancement depicted by conventional magnetic resonance imaging.

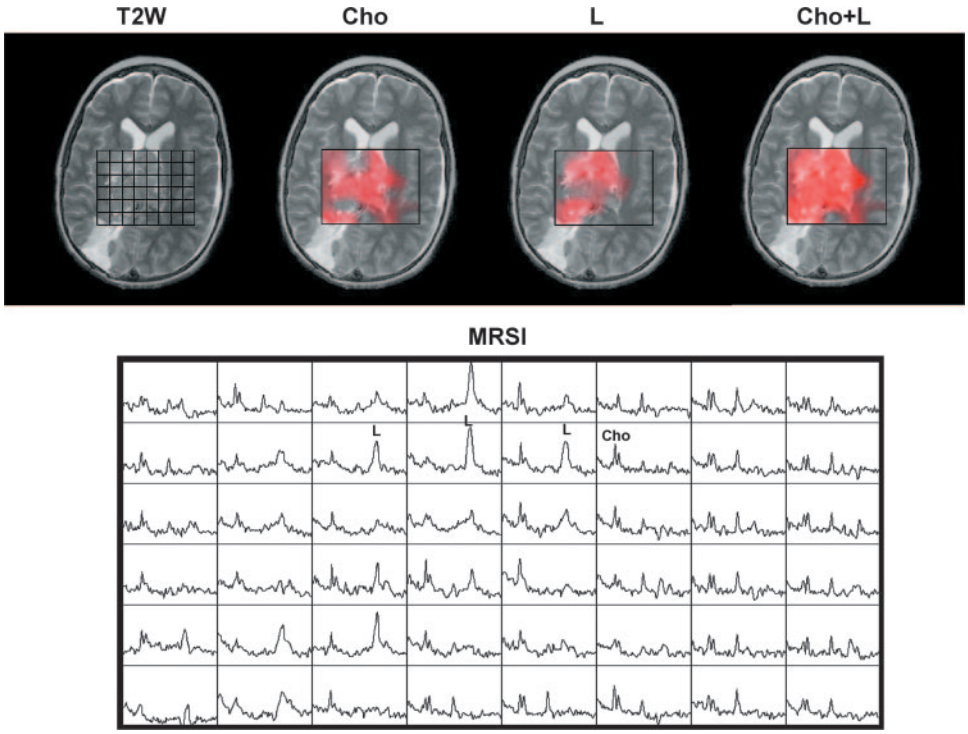

Fig. 2 Magnetic resonance imaging and proton magnetic resonance spectroscopic imaging (MRSI) on an 8-year-old boy with anaplastic astrocytoma of the right thalamus. The axial T2-weighted (T2W) image shows a heterogeneous right thalamic mass extending into the right lateral ventricle and across the midline to the left lateral ventricle. Normalized choline (Cho) and normalized lipids and/or lactate (L) metabolic maps, overlaid on the T2W image, indicate increased Cho and L throughout the lesion, consistent with an active tumor. The combined (Cho + L) biomarker image suggests more extensive tumor involvement than the metabolite images (Cho or L) images alone.

normality, and Cho distribution in a low-grade tumor. Clearly, elevated Cho identifies tumor regions not indicated by the contrast enhancement on the T1-weighted image. At a similar axial level, Fig. 2 illustrates images of a different child with a high-grade tumor, the distribution of Cho and lipids and/or lactate due to mobile lipids and lactate, and the sum of Cho + lipids and/or lactate derived from spectra dominated by high Cho and lipids and/or lactate peaks. Here, the Cho + lipids and/or lactate image is seen to accurately depict the extensive tumor infiltration.

Highly significant median differences for Cho as a continuous variable between low-grade (0.93; range, 0.14 to 2.19) and high-grade (1.70; range, 1.00 to 4.54) tumors are shown by the Mann-Whitney U test ($P < 0.001$), as shown in Fig. 3. Similarly, highly significant median differences in lipids and/or lactate are observed between low-grade (0.0; range, 0 to 3.34) and high-grade (2.75; range, 0 to 9.58) tumors ($P < 0.001$). Indeed, multiple stepwise logistic regression analysis reveals that both biomarkers are significant independent predictors of tumor grade ($P < 0.001$; Table 2). The adjusted odds ratio indicates that a unit increase in Cho is associated with a 25-fold increase in the odds of a high-grade tumor. In addition, the odds of a high-grade tumor are over four times higher for each unit increase in lipids and/or lactate. The Hosmer-Lemeshow test revealed no significant departure from good model fit to the data ($P = 0.84$). The logistic regression model also provides estimated probabilities of a high-grade tumor based on Cho and lipids and/or lactate (L) values ranging from 0 to 5 (Fig. 4). Specifically, if P (high-grade Cho, lipids and/or lactate) denotes the probability of a high-grade tumor given the Cho and L values, then according to the logistic model, P (high-grade Cho, lipids and/or lactate) $= 1/[1 + \exp(-(6.94 + 3.21\text{Cho} + 1.5\text{L})]$. For example, when Cho = 2.0 and lipids and/or lactate = 1.0, P (high-grade tumor) = 0.725 or 72.5%. The surface-plot in Fig. 4 shows that the probability of a high-grade tumor approaches 1 (certainty) for increasing values of Cho and/or lipids and/or lactate.

The distribution-free approach of Pepe and Thomas (32) reveals that the combination of biomarkers that maximizes the area under the ROC curve is Cho + 0.49 L. Fig. 5 presents ROC curves for each separate biomarker and for their linear combination and shows that L (AUC = 0.89) discriminates high- from low-grade tumors better than does Cho (AUC = 0.87). The combined index demonstrates even better accuracy (AUC = 0.97; Table 3), and the AUC for the combined index is significantly higher than for lipids and/or lactate alone ($Z = 1.98$, $P < 0.05$).

Finally, we tested the ability of each biomarker to classify tumor grade by choosing cutoff points corresponding to their maximum accuracy (Table 4) and found that the combined marker was more accurate (91%) than either Cho or lipids and/or lactate alone, more sensitive (96%) than Cho alone, and equally specific as lipids (88%). Fig. 6 visually presents these results, where the combined index cutoff point corresponds to a line in the Cho-lipids and/or lactate plane.

DISCUSSION

Cho and Lipids and/or Lactate Peaks As Novel Magnetic Resonance Spectroscopic Imaging Biomarkers for Tumor Evaluation. This study investigates the utility of proton magnetic resonance spectroscopic imaging in the identification

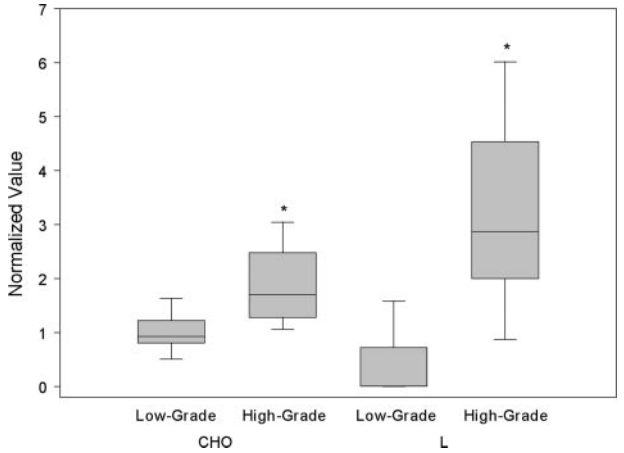

Fig. 3 Box plots illustrating that both normalized values of choline (Cho) and lipids/lactate (L) differentiate high-grade ($n = 23$) *versus* low-grade ($n = 43$) tumors. The limits of the box represent the lower quartile (25th percentile) and upper quartile (75th percentile); the length of the box height is the interquartile range. The top and bottom whiskers are 1.5*interquartile range distance far from the box limits, or they represent the maximum and minimum value, respectively. The median is displayed as the line dividing the box. A significantly higher median Cho is observed in the high-grade tumors (median, 1.7; interquartile range, 1.28 to 2.48; range, 1.00 to 4.54) *versus* the low-grade tumors (median, 0.93; interquartile range, 0.81 to 1.22; range, 0.14 to 2.19; $P < 0.001$, Mann-Whitney U test). Similarly, L exhibits higher values in the high-grade (median, 2.75; interquartile range, 2.01 to 4.44; range, 0 to 9.58) *versus* the low-grade tumors (median, 0; interquartile range, 0 to 0.72; range, 0 to 3.34; $P < 0.001$, Mann-Whitney U test).

of brain tumor biomarkers and provides several significant conclusions for the utility of Cho and lipids and/or lactate, two noninvasive biomarkers, for the improved clinical evaluation of pediatric brain tumors. Importantly, these two biomarkers can serve as independent predictors of tumor grade, and their combination can enhance pediatric brain tumor classification. Tumor grading is essential for optimum therapy, especially for pediatric brain tumors, which in contrast to adult brain tumors have better prognosis, but are often surgically challenging (9). Although both Cho and lipids and/or lactate have previously been associated with tumor grade (36–38), this is the first analysis of their combined utility for pediatric brain tumor assessment.

This study also shows that the region of the magnetic resonance spectroscopic imaging spectrum that has the highest Cho output strongly correlates with the pathological evaluation of the most malignant areas of tumor biopsy specimens, even in cases where the pathology and magnetic resonance spectroscopic imaging resolutions are different. Thus, Cho analysis holds the promise of being able to direct biopsy to regions suitable for additional focal therapy (39); the Cho and lipids and/or lactate peaks can serve as biomarkers to promote treatment tailored to tumor behavior (40); a strong relationship exists between the levels of the magnetic resonance spectroscopic predictors and histopathological evaluation (41). For instance, Cho and lipids and/or lactate peaks are both significant independent predictors of tumor grade and therefore can and should be included in future classification systems of tumor grade. These conclusions are supported, in part, by previous studies showing the potential of magnetic resonance spectroscopic imaging in the differential diagnosis (6, 42) and prognosis (37, 43, 44) of brain tumors.

We note that Fig. 5 reveals two important differences between the Cho and lipids and/or lactate peaks for tumor grade differentiation: the lipids and/or lactate peaks appear more accurate than those for Cho, as indicated by their AUC values (Table 3), and the lipids and/or lactate and the Cho peaks are comparatively more sensitive at the low (high specificity) and the high (low specificity) false positive rate ranges, respectively. Thus, the combined biomarkers provide increased accuracy throughout the false positive rate.

Cho Metabolites. Our results show the prognostic significance of the Cho and lipid peaks, and the relevant biological roles of their underlying respective metabolites additionally supports their significance for brain tumor assessment. For example, we show that high-grade tumors that are highly cellularized and have high proliferative potential contain regions with increased Cho levels *versus* normal brain tissue. Cho peaks are elevated in actively proliferating cells, as measured by phosphorous or proton magnetic resonance spectroscopic imaging, and *in vivo* proton magnetic resonance spectroscopic imaging suggests that Cho peaks correlate with proliferative activity in gliomas (43, 44). The *in vivo* Cho peak actually has three constituents, phosphocholine (PCho), glycerophosphocholine, and free choline (45), with the PCho levels all thought to be related to cell proliferation or growth stimulation and associated with oncogenic and malignant transformation (15). PCho appears to play a role in carcinogenesis because choline kinase, the enzyme that converts Cho into PCho, is overexpressed in several human cancers (46). Unfortunately, 1.5-Tesla magnetic field strength instruments, as well as 3- and 4-Tesla systems recently approved for clinical use, are as yet unable to resolve the *in vivo* Cho peak constituents. The future development of this ability could prove of great clinical use to evaluate specific Cho metabolites and therapeutic response in cancer patients.

The PCho-dominated Cho signal likely also reflects levels of local cellularity (47, 48). The Cho peak detected by *in vivo* magnetic resonance spectroscopic is likely elevated because the volume of interest is either highly cellular (47, 48), includes

Table 2 Multivariate analysis: independent predictors of tumor grade

Predictor	Regression (slope) coefficient (SE)	Adjusted odds ratio (95% CI)	Likelihood ratio test *	*P*
Cho	3.21 (1.12)	24.8 (2.7–225)	13.1	<0.001
L	1.50 (0.42)	4.4 (2.0–10.1)	25.0	<0.001

NOTE. Constant term (intercept) = −6.94.
Abbreviation: CI, confidence interval.
* Test statistic obtained from logistic regression analysis that follows a chi-square distribution with 1 degree of freedom.

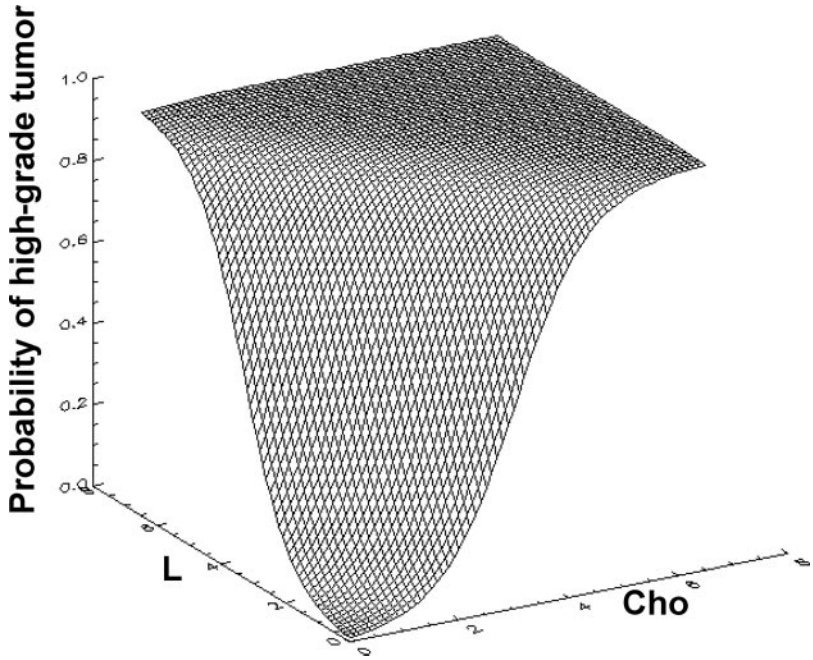

Fig. 4 Surface-plot calculated from the estimated probability, according to a logistic regression model of high-grade tumor based on levels of normalized choline (Cho) and lipid or lactate (L), ranging from 0 to 5. In the three-dimensional graph, a highly significant positive relationship between both Cho and L and high-grade tumor ($P < 0.001$) is shown as the surface-plot tends to probability values equal to 1 for increasing Cho and/or L values.

high PCho cells due to their increased proliferative potential (49–52), or includes oncogenically and malignantly transformed cells (15).

Lipid and/or Lactate Metabolites. The lipid and/or lactate peaks detected here consist primarily of lipids and secondarily of lactate because our methodology is sensitized for lipid *versus* lactate. We note in contrast that Garwood *et al.* (16, 53) tailored their approach to lactate detection and showed that this metabolite is an indicator of tumor metabolic activity, a role that has received both positive (6) and negative (54, 55) support. We believe the utility of lactate as an *in vivo* magnetic resonance spectroscopic predictor in the clinical setting can only be ascertained upon implementation of appropriate methods for its detection (56, 57).

Our analysis reveals that increased lipid and/or lactate peak levels predict high-grade brain tumors, which are generally highly necrotic. To this end, magnetic resonance spectroscopic visible lipids correlate with apoptosis (58), necrosis (26), and with the proportion of cells in S and G_2 phase (59). Furthermore, gene therapy-induced apoptosis of experimental gliomas correlates with substantial accumulation of proton magnetic resonance spectroscopic visible polyunsaturated fatty acids (60, 61), and magnetic resonance spectroscopic studies of necrotic tissue show the polyunsaturated fatty acids and other lipids remain visible in the late stages of apoptosis to suggest that lipid bodies remain after cell death (61). We therefore anticipate that magnetic resonance spectroscopic of tumor biopsies, combined with histopathology, should show that the magnetic resonance spectroscopic visible lipid peak correlates with necrosis, which standard histology may be unable to differentiate from late stage apoptosis. Such a correlation could be borne out by studies of magnetic resonance spectroscopic visible lipids *versus* apoptotic bodies detected by terminal deoxynucleotidyl transferase-mediated nick end labeling. Nonetheless, our results to date suggest a time-window occurs during cell death when magnetic resonance spectroscopic visible lipid resonances are dynamic, which could provide useful prognostic information.

Pattern Recognition. Our combinatorial approach provides a novel solution for pattern recognition that overcomes the limitations of trying to optimize for both sensitivity and speci-

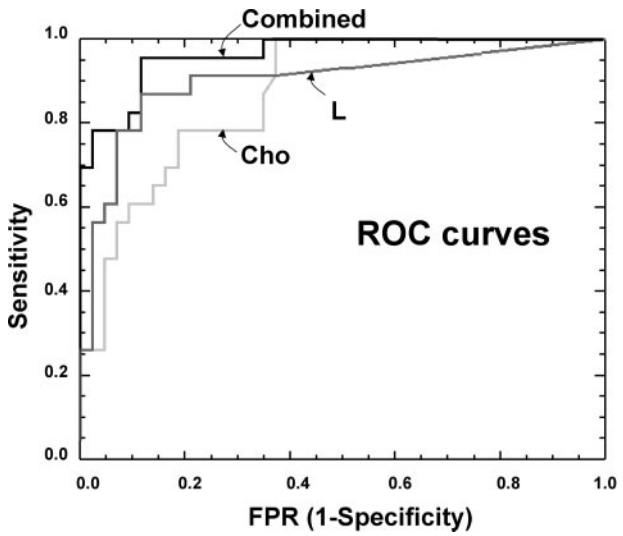

Fig. 5 ROC curves for normalized choline (Cho, *gray*), normalized lipid or lactate (L, *charcoal*), and for the linear combined model (*black*). AUC is a measure of the average accuracy of a statistical test. A perfect test has an AUC of 1.0, whereas a test with chance level discrimination has a ROC area of 0.5. L (AUC = 0.89) discriminates high- from low-grade tumors better than Cho (AUC = 0.87). The combined index has an even significantly better level of accuracy than the biomarkers separately (AUC = 0.97). FPR, false positive rate.

Table 3 Areas under the ROC curves

Biomarker	AUC	SE	95% CI
Cho	0.87	0.04	0.79–0.75
L	0.89	0.04	0.81–0.97
Combined	0.97	0.02	0.93–1.00

Abbreviations: AUC, area under the curve; CI, confidence interval.

ficity. Previous studies have classified brain tumor grade with magnetic resonance spectroscopic biomarkers and pattern recognition algorithms (62–68). To this end, Preul *et al.* (6) reported 99% accuracy with a linear discriminant analysis and values based on six metabolites, whereas Arle *et al.* (69) reported 95% accuracy with neuronal networks algorithms on data combining magnetic resonance spectroscopic and clinical markers. We emphasize here the utility of Cho and lipid and/or lactate in brain tumor grading in inoperable clinical cases. As a measure of accuracy, we have chosen the area under the ROC curve, the most widely used index of diagnostic accuracy for diagnostic tests with continuous or ordinal data (70). This allows us to construct a combined biomarker without choosing a specific decision rule or cutoff point.

Other classification algorithms applied in tumor classification such as linear discriminant analysis (6, 62, 63), neuronal networks (64, 66, 69), cluster analysis (71), and binary decision trees (67) derive specific decision rules to optimize their objective function. In contrast, our distribution free approach provides a combined diagnostic test with the ability to choose cutoff points according to the most suitable sensitivity and specificity. To best derive specific cutoff points, information for both the decision cost and the disease prevalence need be considered (72). For example, where environmental factors have increased the prevalence of high-grade tumors, a cutoff point with increased sensitivity and decreased specificity is called for, whereas a cutoff point with increased specificity and decreased sensitivity is called for when using a novel therapy that has beneficial effects to high-grade tumors and significant side effects to low-grade tumors. Our combined biomarker approach can be used in both these cases because it uses the AUC measure, which does not depend on disease prevalence nor the cost of a false decision. Hence, the Table 4 cutoff points, which represent optimal operating points of maximum accuracy, are essentially arbitrary and only representative examples. Similarly, the line drawn in Fig. 6 corresponds to a single cutoff point of maximum accuracy and can be moved parallel if a different sensitivity or specificity is required.

Current Limitations and Future Directions. The improved classification depicted in Fig. 6 is still imperfect because the high- and low-grade tumor populations are intermixed and cannot be completely separated on the Cho-lipid and/or lactate plane, regardless of the classification algorithm. Several explanations can account for the potential false positives or negatives in the magnetic resonance spectroscopic imaging data. False positives can be produced when a low-grade tumor is metabolically active and has elevated lactate, quantification fails to discriminate baseline effects in short echo time spectra from lipid peaks, or an undetected artifact such as voxel bleeding alters the real metabolic profile of the tissue. False negatives can be produced when regions of biopsy sampling differ from the highest choline regions or the tumor has high heterogeneity. Methods that take these limitations into account and thus hold promise to improve magnetic resonance spectroscopic imaging performance to classify tumor grade include coverage of larger areas with three-dimensional chemical shift imaging, smaller voxel volumes, higher magnetic fields, improved scalp lipid suppression, and faster acquisition sequences. Also, magnetic resonance spectroscopic imaging, although providing unique metabolic insights into the tumor tissue, has inherently low sensitivity and may be combined with other modalities and clinical markers for finest diagnostic accuracy. To this end, DNA microarray-based gene expression profiling can be more sensitive than histopathological evaluation for tumor classification (4). Such profiling may indeed prove to correlate better with magnetic resonance spectroscopic imaging biomarkers such as those identified here and in the future come to replace current histopathology techniques to evaluate pediatric brain tumors and their course of treatment.

Table 4 Diagnostic characteristics of biomarkers with cutoff points at maximum accuracy in differentiating high-grade and low-grade tumors

Biomarker	Cutoff point	Sensitivity (%)	Specificity (%)	Accuracy (%)	Likelihood ratio*
Cho	1.25	78 (18/23)	81 (35/43)	80 (53/66)	4.1
L	1.10	87 (20/23)	88 (38/43)	88 (58/66)	7.3
Combined	1.80	96 (22/23)	88 (38/43)	91 (60/66)	8.0

* Defined as sensitivity/(one-specificity). This represents the ratio of the likelihood of a positive test result for biomarkers (above cutoff point) in someone with high-grade tumor to the likelihood of that result in someone with a low-grade tumor.

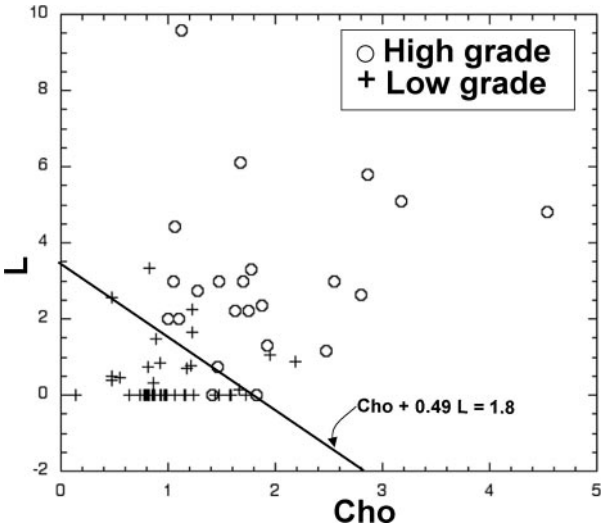

Fig. 6 Graph of normalized choline (Cho) *versus* lipid or lactate (L) levels, measured in patients with high-grade (○) and low-grade (+) tumors. The line Cho + 0.49 L = 1.8 corresponds to a cutoff point 1.8 for the combined biomarker estimated with a distribution-free approach (32). Note that by moving this line parallel to its self, the cutoff points are varied, whereas the combined biomarker remains unchanged.

This study explores the potential of using proton magnetic resonance spectroscopic imaging to provide reproducible diagnostic and prognostic biomarkers to evaluate tumor biology and metabolism. Such biomarkers could greatly aid in the choice of treatment of pediatric brain tumors and influence decisions to adjust therapy before the onset of toxicity. Our results suggest that normalized Cho and lipids and/or lactate can serve as independent prognostic indices of tumor grading and moreover can be linearly combined to create an accurate noninvasive diagnostic test for any required sensitivity or specificity. This multiparametric biomarker approach is a promising methodology to improve the diagnosis, prognosis, and development of therapies tailored to tumor behavior, especially when obtaining a biopsy is not feasible.

ACKNOWLEDGMENTS

We thank the Departments of Radiology, Neurosurgery and Pathology at Children's Hospital (Boston, MA) for supporting this study, and Dr. Scott Stachel for comments on the manuscript and editing.

REFERENCES

1. Pollack I. Brain tumors in children. N Engl J Med 1994;331:1500–7.

2. Kim JY, Sutton ME, Lu DJ, et al. Activation of neurotrophin-3 receptor TrkC induces apoptosis in medulloblastomas. Cancer Res 1999;59:711–9.

3. Chakravarti A, Noll E, Black PM, et al. Quantitatively determined survivin expression levels are of prognostic value in human gliomas. J Clin Oncol 2002;20:1063–8.

4. Pomeroy SL, Tamayo P, Gaasenbeek M, et al. Prediction of central nervous system embryonal tumour outcome based on gene expression. Nature (Lond) 2002;415:436–42.

5. Nutt CL, Mani DR, Betensky RA, et al. Gene expression-based classification of malignant gliomas correlates better with survival than histological classification. Cancer Res 2003;63:1602–7.

6. Preul MC, Caramanos Z, Collins DL, et al. Accurate, noninvasive diagnosis of human brain tumors by using proton magnetic resonance spectroscopy. Nat Med 1996;2:323–5.

7. Wald LL, Nelson SJ, Day MR, et al. Serial proton magnetic resonance spectroscopy imaging of glioblastoma multiforme after brachytherapy. J Neurosurg 1997;87:525–34.

8. Tzika AA, Vajapeyam S, Barnes PD. Multivoxel proton MR spectroscopy and hemodynamic MR imaging of childhood brain tumors: preliminary observations. AJNR:Am J Neuroradiol 1997;18:203–18.

9. Lazareff JA, Bockhorst KH, Curran J, Olmstead C, Alger JR. Pediatric low-grade gliomas: prognosis with proton magnetic resonance spectroscopic imaging. Neurosurgery 1998;43:809–17.

10. Gupta RK, Cloughesy TF, Sinha U, et al. Relationships between choline magnetic resonance spectroscopy, apparent diffusion coefficient and quantitative histopathology in human glioma. J Neurooncology 2000;50:215–26.

11. Tzika A, Astrakas L, Kieran M, Zurakowski D, Zarifi M, Poussaint T. Choline to n-acetylaspartate ratio is predictive of pediatric brain tumor progression. Radiology 2001;221(Suppl):488.

12. Tzika AA, Zarifi MK, Goumnerova L, et al. Neuroimaging in pediatric brain tumors: Gd-DTPA–enhanced, hemodynamic, and diffusion MR imaging compared with MR spectroscopic imaging. AJNR Am J Neuroradiol 2002;23:322–33.

13. Tzika AA, Astrakas LG, Zarifi MK, et al. Multiparametric MR assessment of pediatric brain tumors. Neuroradiology 2003;45:1–10.

14. Podo F. Tumour phospholipid metabolism. NMR Biomed 1999;12:413–39.

15. Ackerstaff E, Pflug BR, Nelson JB, Bhujwalla ZM. Detection of increased choline compounds with proton nuclear magnetic resonance spectroscopy subsequent to malignant transformation of human prostatic epithelial cells. Cancer Res 2001;61:3599–603.

16. Terpstra M, Gruetter R, High WB, et al. Lactate turnover in rat glioma measured by in vivo nuclear magnetic resonance spectroscopy. Cancer Res 1998;58:5083–8.

17. Tallan HH. Studies on the distribution of N-acetyl-L-aspartic acid in brain. J Biol Chem 1957;224:41–5.

18. Koller KJ, Zaczek R, Coyle JT. N-Acetyl-aspartyl-glutamate: regional levels in rat brain and the effects of brain lesions as determined by a new HPLC method. J Neurochem 1984;43:1136–42.

19. Urenjak J, Williams SR, Gadian DG, Noble M. Proton nuclear magnetic resonance spectroscopy unambiguously identifies different neural cell types. J Neurosci 1993;13:981–9.

20. Noble M, Gutowski N, Bevan K, et al. From rodent glial precursor cell to human glial neoplasia in the oligodendrocyte-type-2 astrocyte lineage. Glia 1995;15:222–30.

21. Hakumaki JM, Poptani H, Puumalainen AM, et al. Quantitative 1H nuclear magnetic resonance diffusion spectroscopy of BT4C rat glioma during thymidine kinase-mediated gene therapy in vivo: identification of apoptotic response. Cancer Res 1998;58:3791–9.

22. Lahrech H, Zoula S, Farion R, Remy C, Decorps M. In vivo measurement of the size of lipid droplets in an intracerebral glioma in the rat. Magn Reson Med 2001;45:409–14.

23. Kauppinen RA. Monitoring cytotoxic tumour treatment response by diffusion magnetic resonance imaging and proton spectroscopy. NMR Biomed 2002;15:6–17.

24. Blankenberg FG, Katsikis PD, Storrs RW, et al. Quantitative analysis of apoptotic cell death using proton nuclear magnetic resonance spectroscopy. Blood 1997;89:3778–86.

25. Kuesel AC, Donnelly SM, Halliday W, Sutherland GR, Smith IC. Mobile lipids and metabolic heterogeneity of brain tumors as detectable by ex vivo 1H MR spectroscopy. NMR in Biomedicine 1994;7:172–80.

26. Tzika AA, Cheng LL, Goumnerova L, et al. Biochemical characterization of pediatric brain tumors by using in vivo and ex vivo magnetic resonance spectroscopy. J Neurosurg 2002;96:1023–31.

27. Tzika A, Astrakas L, Zurakowski D, et al. Predicting clinical grade of CNS tumors in children with non-invasive magnetic resonance spectroscopic imaging [abstract]. In: 94th Annual Meeting of the American Association for Cancer Research, Washington, D.C., July 2003. Proc Am Assoc Cancer Res 2003;44:680.

28. Bottomley PA. Selective volume method for performing localized NMR spectroscopy. United States patent US4480228. Assignee General Electric Company, Schenectady, NY, 1984.

29. Nelson SJ, Brown TR. A new method for automatic quantification of 1-D spectra with low signal to noise ratio. J Magn Reson 1987;75:229–43.

30. Weinstein M, Fineberg H. Clinical decision analysis. Philadelphia, PA: W. B. Saunders; 1980. p. 114–27.

31. Hosmer DW, Lemeshow S. Applied logistic regression, 2nd ed. New York: John Wiley & Sons; 2000. p. 34–57.

32. Pepe MS, Thompson ML. Combining diagnostic test results to increase accuracy. Biostatistics 2000;1:123–40.

33. Obuchowski NA. Receiver operating characteristic curves and their use in radiology. Radiology 2003;229:3–8.

34. Hanley JA, McNeil BJ. The meaning and use of the area under a receiver operating characteristic (ROC) curve. Radiology 1982;143:29–36.

35. Hanley JA, McNeil BJ. A method of comparing the areas under receiver operating characteristic curves derived from the same cases. Radiology 1983;148:839–43.

36. Gill SS, Thomas DGT, Van Bruggen N, et al. Proton MR spectroscopy of intracranial tumours: in vivo and in vitro studies. J Comput Assist Tomogr 1990;14:497–504.

37. Poptani H, Gupta RK, Roy R, Pandey R, Jain VK, Chhabra DK. Characterization of intracranial mass lesions with in vivo proton MR spectroscopy. AJNR Am J Neuroradiol 1995;16:1593–603.

38. Howe FA, Barton SJ, Cudlip SA, et al. Metabolic profiles of human brain tumors using quantitative in vivo 1H magnetic resonance spectroscopy. Magn Reson Med 2003;49:223–32.

39. Pirzkall A, McKnight TR, Graves EE, et al. MR-spectroscopy guided target delineation for high-grade gliomas. Int J Radiat Oncol Biol Phys 2001;50:915–28.

40. Li X, Lu Y, Pirzkall A, McKnight T, Nelson SJ. Analysis of the spatial characteristics of metabolic abnormalities in newly diagnosed glioma patients. J Magn Reson Imaging 2002;16:229–37.

41. McKnight TR, von dem Bussche MH, Vigneron DB, et al. Histopathological validation of a three-dimensional magnetic resonance spectroscopy index as a predictor of tumor presence. J Neurosurg 2002;97:794–802.

42. Nelson SJ, Vigneron DB, Dillon WP. Serial evaluation of patients with brain tumors using volume MRI and 3D 1H MRSI. NMR Biomed 1999;12:123–38.

43. Shimizu H, Kumabe T, Shirane R, Yoshimoto T. Correlation between choline level measured by proton MR spectroscopy and Ki-67 labeling index in gliomas. AJNR Am J Neuroradiol 2000;21:659–65.

44. Tamiya T, Kinoshita K, Ono Y, Matsumoto K, Furuta T, Ohmoto T. Proton magnetic resonance spectroscopy reflects cellular proliferative activity in astrocytomas. Neuroradiology 2000;42:333–8.

45. Barker P, Breiter S, Soher B, et al. Quantitative proton spectroscopy of canine brain: in vivo and in vitro correlations. Magn Reson Med 1994;32:157–63.

46. Ramirez de Molina A, Rodriguez-Gonzalez A, Gutierrez R, et al. Overexpression of choline kinase is a frequent feature in human tumor-derived cell lines and in lung, prostate, and colorectal human cancers. Biochem Biophys Res Commun 2002;296:580–3.

47. Miller BL, Chang L, Booth R, et al. In vivo 1H MRS choline: correlation with in vitro chemistry/histology. Life Sci 1996;58:1929–35.

48. Chang L, McBride D, Miller BL, et al. Localized in vivo 1H magnetic resonance spectroscopy and in vitro analyses of heterogeneous brain tumors. J Neuroimaging 1995;5:157–63.

49. Daly PF, Lyon RC, Faustino PJ, Cohen JS. Phospholipid metabolism in cancer cells monitored by 31P NMR spectroscopy. J Biol Chem 1987;262:14875–8.

50. Gillies RJ, Barry JA, Ross BD. In vitro and in vivo 13C and 31P NMR analyses of phosphocholine metabolism in rat glioma cells. Magn Reson Med 1994;32:310–8.

51. Aiken NR, Szwergold ES, Kappler F, et al. Metabolism of phosphonium choline by rat-2 fibroblasts: effects of mitogenic stimulation studied using 31P NMR spectroscopy. Anticancer Res 1996;16:1357–63.

52. Mahmood U, Alfieri AA, Thaler H, Cowburn D, Koutcher JA. Radiation dose-dependent changes in tumor metabolism measured by 31P nuclear magnetic resonance spectroscopy. Cancer Res 1994;54:4885–91.

53. Ross BD, Merkle H, Hendrich K, Staewen RS, Garwood M. Spatially localized in vivo 1H magnetic resonance spectroscopy of an intracerebral rat glioma. Magn Reson Med 1992;23:96–108.

54. Fulham MJ, Bizzi A, Dietz MJ, Shih HH, Raman R. Mapping of brain tumor metabolites with proton MR spectroscopic imaging: clinical relevance. Radiology 1992;185:675–86.

55. Kugel H, Heindel W, Ernestus RI, Bunke J, du Mesnil R, Friedman G. Human brain tumors: spectral patterns detected with localized H-1 MR spectroscopy. Radiology 1992;183:701–9.

56. Duyn JH, Frank JA, Moonen CT. Incorporation of lactate measurement in multi-spin-echo proton spectroscopic imaging. Magn Reson Med 1995;33:101–7.

57. Thomas MA, Ryner LN, Mehta MP, Turski PA, Sorenson JA. Localized 2D J-resolved 1H MR spectroscopy of human brain tumors in vivo. J Magn Reson Imaging 1996;6:453–59.

58. Blankenberg FG, Storrs RW, Naumovski L, Goralski T, Spielman D. Detection of apoptotic cell death by proton nuclear magnetic resonance spectroscopy. Blood 1996;87:1951–6.

59. Veale MF, Roberts NJ, King GF, King NJ. The generation of 1H-NMR-detectable mobile lipid in stimulated lymphocytes: relationship to cellular activation, the cell cycle, and phosphatidylcholine-specific phospholipase C. Biochem Biophys Res Commun 1997;239:868–74.

60. Hakumaki JM, Poptani H, Sandmair AM, Yla-Herttuala S, Kauppinen RA. 1H MRS detects polyunsaturated fatty acid accumulation during gene therapy of glioma: implications for the in vivo detection of apoptosis. Nat Med 1999;5:1323–7.

61. Griffin JL, Lehtimaki KK, Valonen PK, et al. Assignment of 1H nuclear magnetic resonance visible polyunsaturated fatty acids in BT4C gliomas undergoing ganciclovir-thymidine kinase gene therapy-induced programmed cell death. Cancer Res 2003;63:3195–201.

62. De Edelenyi FS, Rubin C, Esteve F, et al. A new approach for analyzing proton magnetic resonance spectroscopic images of brain tumors: nosologic images. Nat Med 2000;6:1287–9.

63. Tate AR, Majos C, Moreno A, Howe FA, Griffiths JR, Arus C. Automated classification of short echo time in in vivo 1H brain tumor spectra: a multicenter study. Magn Reson Med 2003;49:29–36.

64. Usenius JP, Tuohimetsa S, Vainio P, Ala-Korpela M, Hiltunen Y, Kauppinen RA. Automated classification of human brain tumours by neural network analysis using in vivo 1H magnetic resonance spectroscopic metabolite phenotypes. Neuroreport 1996;7:1597–600.

65. De Stefano N, Caramanos Z, Preul MC, Francis G, Antel JP, Arnold DL. In vivo differentiation of astrocytic brain tumors and isolated demyelinating lesions of the type seen in multiple sclerosis using 1H magnetic resonance spectroscopic imaging. Ann Neurol 1998;44:273–8.

66. Poptani H, Kaartinen J, Gupta RK, Niemitz M, Hiltunen Y, Kauppinen RA. Diagnostic assessment of brain tumours and non-neoplastic brain disorders in vivo using proton nuclear magnetic resonance spectroscopy and artificial neural networks. J Cancer Res. Clin Oncol 1999;125:343–9.

67. Majos C, Alonso J, Aguilera C, et al. Adult primitive neuroectodermal tumor: proton MR spectroscopic findings with possible application for differential diagnosis. Radiology 2002;225:556–66.

68. Howe FA, Opstad KS. 1H MR spectroscopy of brain tumours and masses. NMR Biomed 2003;16:123–31.

69. Arle JE, Morriss C, Wang ZJ, Zimmerman RA, Phillips PG, Sutton LN. Prediction of posterior fossa tumor type in children by means of magnetic resonance image properties, spectroscopy, and neural networks. J Neurosurg 1997;86:755–61.

70. Begg CB. Advances in statistical methodology for diagnostic medicine in the 1980's. Stat Med 1991;10:1887–95.

71. Jacobs MA, Barker PB, Bluemke DA, et al. Benign and malignant breast lesions: diagnosis with multiparametric MR imaging. Radiology 2003;229:225–32.

72. Zweig MH, Campbell G. Receiver-operating characteristic (ROC) plots: a fundamental evaluation tool in clinical medicine. Clin Chem 1993;39:561–77.

Clinical Cancer Research

Noninvasive Magnetic Resonance Spectroscopic Imaging Biomarkers to Predict the Clinical Grade of Pediatric Brain Tumors

Loukas G. Astrakas, David Zurakowski, A. Aria Tzika, et al.

Clin Cancer Res 2004;10:8220-8228.